Chemical Engineering Journal 103 (2004) 133–145

Chemical Engineering Journal

www.elsevier.com/locate/cej

Intraparticle diffusion in single and multicomponent acid dye adsorption from wastewater onto carbon

Keith K.H. Choy, John F. Porter, Gordon Mckay*

Department of Chemical Engineering, Hong Kong University of Science and Technology, Clear Water Bay, Kowloon, Hong Kong, PR China

Received 31 January 2004; received in revised form 22 April 2004; accepted 25 May 2004

Abstract

The adsorption of three acid dyes onto activated carbon has been studied. Three single, three binary and one ternary systems have been investigated and both equilibrium and kinetic studies have been determined. The equilibrium capacities based on the Langmuir analysis are 0.253, 0.125 and 0.219 mmol g^{-1} carbon for Acid Blue 80, Acid Red 114 and Acid Yellow 117, respectively. The batch adsorber rate data for the seven systems have been analysed based on an intraparticle diffusion rate parameter derived from the plots of dye adsorbed versus the square root of time. The data indicate the adsorption mechanism is predominantly intraparticle diffusion. The multicomponent system rate parameters have been correlated with the single component rate parameters by the use of the Langmuir equilibrium parameters.

Keywords: Diffusion modelling; Adsorption; Activated carbon; Acid dyes; Multicomponent

1. Introduction

The economic removal of colour from textile industry effluents remains a major problem. Many dyes, although not toxic, present an aesthetic problem and reduce photosynthetic activity in the receiving waters into which they are discharged. Many dyes are designed for their chemical stability and do not undergo biochemical degradation readily. The amount of dyes discharged in the world for the textile industry is about 146,000 tonnes per year [1].

Conventional methods for the removal of dyestuffs from wastewater include adsorption onto solid substrates, chemical coagulation, disinfection, filtration and UV treatment [2–4]. Adsorption has become a well-established separation technique to remove dilute pollutants as well as having the potential for regeneration, recovery and recycling of the adsorbed materials.

Several adsorbents have been studied to determine their ability to adsorb dyes from aqueous effluents, including pith [5], palm-fruit bunch particles [6], peat [7,8], bagasse fly ash [9], wood [10], glass powder [11] and chitosan [12–15]. However, for research purposes the most widely used dye adsorbent and most readily available from commercial sources is activated carbon [16–20]. Consequently an activated carbon has been selected for this study.

There is only limited research data available on multicomponent dye adsorption [21–23], and it is important to develop design models for such practical systems. In the present research, three acid dyes have been selected, namely, Acid Blue 80, Acid Red 114 and Acid Yellow 117, due to their widespread use and high stability, single, binary and ternary component batch adsorption studies have been carried out using different initial dye concentrations and carbon masses. Single and multicomponent equilibrium isotherms have been determined and analysed. An intraparticle diffusion model will been used to test the mechanism and correlate the experimental single and multicomponent data in order to limit the amount of time consuming experimental work required to be performed for system design.

2. Materials and experimental section

2.1. Adsorbent

The adsorbent used in the research was a granular activated carbon (GAC) type F400; it was supplied by Chemviron Carbon Ltd. This carbon was described by the supplier as a generally effective water treatment activated carbon. Activated Carbon Filtrasorb 400 was crushed by using a hammer mill and washed with distilled water to remove fines. Then, the activated carbon was dried at 110 °C in an oven

* Corresponding author. Tel.: +852 2358 7133; fax: +852 2358 0054.
E-mail address: kemckayg@ust.hk (G. Mckay).

1385-8947/$ – see front matter © 2004 Elsevier B.V. All rights reserved.
doi:10.1016/j.cej.2004.05.012

Nomenclature

a_L	Langmuir isotherm constant ($dm^3\,mmol^{-1}$)
C_e	equilibrium liquid-phase concentration ($mmol\,dm^{-3}$)
C_t	liquid-phase concentration at time t ($mmol\,dm^{-3}$)
C_0	initial liquid-phase concentration ($mmol\,dm^{-3}$)
d_p	diameter of sorbent (cm)
D_s	surface diffusivity ($cm^2\,s^{-1}$)
exp	experimental
i	ith component in a multisolute system
k	intraparticle rate parameter ($mmol\,g^{-1}\,min^{-0.5}$)
K_L	Langmuir isotherm constant ($dm^3\,g^{-1}$)
M	weight of adsorbent (g)
multi	multicomponent
P	P-factor
q_e	equilibrium solid-phase concentration ($mmol\,g^{-1}$)
q_t	equilibrium solid-phase concentration at time t ($mmol\,g^{-1}$)
q_∞	equilibrium solid-phase concentration when time equal to infinite ($mmol\,g^{-1}$)
q_{max}	monolayer capacity of Langmuir equation ($mmol\,g^{-1}$)
r	radius of sorbent (cm)
SSE	sum of the squares of the error
t	time (min)
theo	theoretical
T	temperature (K)
V	liquid-phase volume (dm^3)
0	single component

Greek letters

λ_{max}	maximum absorption wavelength (nm)
ρ	particle density ($g\,cm^{-3}$)

for 24 h. The 500–710 μm size range activated carbon was sieved out and used for all the experiments in this study. The carbon particles were assumed to be spheres having a diameter given by the arithmetic mean value between respective mesh sizes (average particle diameter, d_p, was 605 μm). The particles appeared irregularly shaped under a microscope but approximated more closely to spheres than to cylinders or parallel pipes for the size ranges under investigation. Table 1 gives the physical properties of carbon F400.

Table 1
Physical properties of activated carbon Filtrasorb 400

Total surface (N_2 BET method) ($m^2\,g^{-1}$)	1150
Bed density, backwashed and drained ($kg\,m^{-3}$)	425×10^3
Particle density ($g\,cm^{-3}$)	1.30
Particle voidage fraction	0.38

Table 2
Information regarding the acid dyes

Name of dyes	AB80	AR114	AY117
Color index number	61585	23635	24820
Molar mass ($g\,mol^{-1}$)	676	830	848
Dye content (%)	60	45	60
λ_{max} (nm)	626	522	438

2.2. Adsorbates

Three dyes, namely Acid Blue 80 (AB80), Acid Red 114 (AR114) and Acid Yellow 117 (AY117), were used in this study. The dyestuffs were used as the commercial salts. AB80 and AY117 were supplied by Ciba Speciality Chemicals and AR114 was supplied by Sigma–Aldrich Chemical Company. Some information regarding the three acid dyes, which were used to measure and prepare standard concentration dye solutions, are listed in Table 2. The data include colour index number, molecular mass, dye content and the wavelengths at which maximum absorption of light occurs, λ_{max}. The structures of three acid dyes are shown in Fig. 1.

2.3. Equilibrium study

The equilibrium isotherms were determined by contacting a constant mass of carbon with a range of dye concentration solutions. A series of fixed volumes (0.050 dm^3) of solutions with predetermined initial dye concentrations were prepared and brought into contact with predetermined masses (0.050 g) of Activated Carbon F400. Therefore, a constant M/V ratio was used throughout the process. The jars were sealed and agitated in the shaker bath (200 rpm shaking rate) at constant temperature $20 \pm 1\,^{\circ}C$ until equilibrium was reached. The bottles were gently agitated for 21 days which was necessary to ensure equilibrium was reached [23]. For the multicomponent systems, all solutions were prepared with solutions of equal mass concentrations. The samples were analysed using a Varian Cary IE spectrophotometer to determine the equilibrium concentration. Three single component systems, AB80, AR114 and AY117, and three binary component systems, AB80 + AR114, AB80 + AY117 and AR114 + AY117, were carried out in the isotherm equilibrium studies.

2.4. Batch kinetic study

These experiments were used to investigate the influence of initial concentration and sorbent mass on the adsorption rate. An adsorber vessel in a batch stirred tank configuration was used in all of the experiments. The design of the standard agitated batch adsorber has been described in previous papers [24,25].

The effect of concentration of acid dye solution on the adsorption rate was studied in these experiments. About 1.7 g

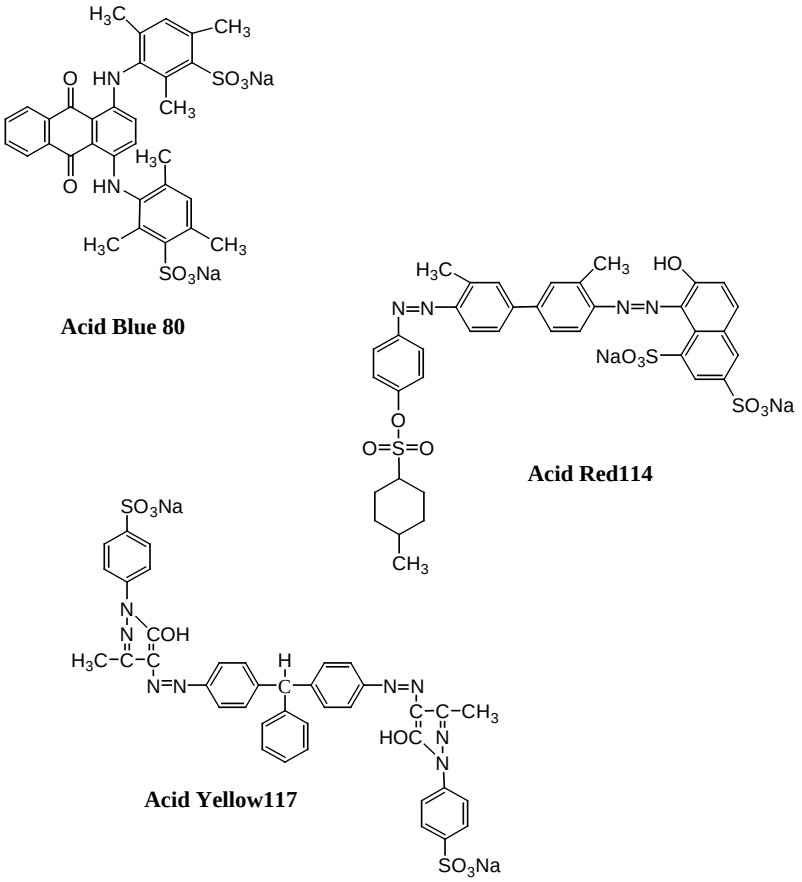

Fig. 1. Dye structures of AR114, AB80 and AY117.

of activated carbon was mixed with 1.7 dm^3 dye solution containing acid dye in the batch system for 12 h. The impeller speed was 400 rpm and the temperature was kept at $20 \pm 1\,^{\circ}C$. A range of concentrations of acid dye solutions (50, 75, 100, 150 and 200 mg dm^{-3}) was used to analyse the sorption of acid dyes onto activated carbon. At time = 0 and at selected time intervals, 3 ml samples were extracted from the adsorption vessel using a 10 ml syringe. The con-

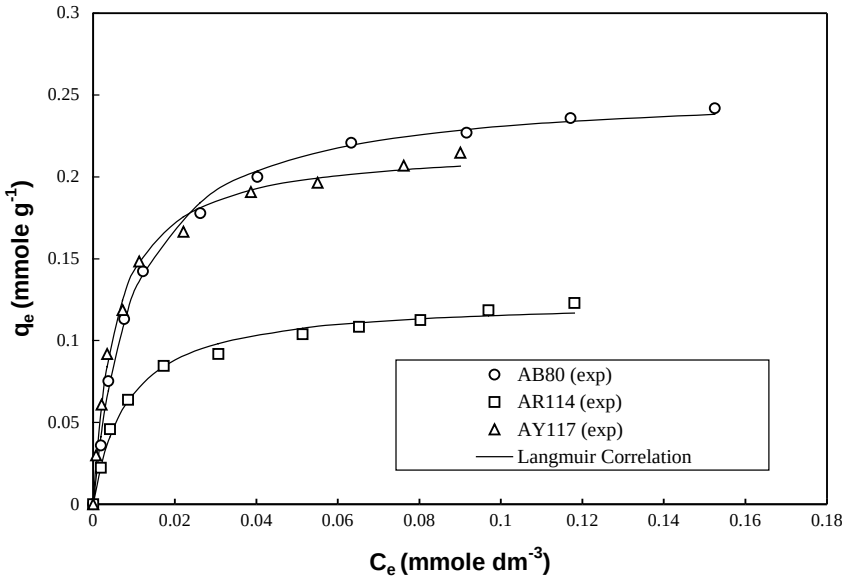

Fig. 2. Langmuir isotherm plots for three acid dyes in a single component systems.

centrations of the dye samples were determined by UV-Vis spectrophotometry.

3. Results and discussion

3.1. Equilibrium isotherm

The equilibrium isotherms for the three single component, three binary component and one ternary component systems have been measured. The experiments were carried out for 21 days which was sufficient to ensure equilibrium has been reached. The isotherm capacity plots are shown in Figs. 2–4 for AB80, AR114 and AY117, respectively for the single, binary and ternary systems. In almost all cases, it can be seen from the figures that a maximum saturation capacity or monolayer is achieved. This suggests that a Langmuir isotherm equation [26] may be applicable to describe each isotherm. The Langmuir equation is shown in Eq. (1):

$$q_{e,i} = \frac{K_{L,i} C_{e,i}}{1 + a_{L,i} C_{e,i}} \quad (1)$$

The Langmuir constants and correlation coefficients were determined by minimising the difference between experimental and theoretical data using the sum of square of error (SSE) (see Eq. (2)) (Table 3):

$$\mathrm{SSE} = \sum_{n=i}^{p} (q_{e,\mathrm{theo}} - q_{e,\mathrm{exp}})_i^2 \quad (2)$$

and the monolayer maximum adsorption capacity, $q_{i,\max}$, is:

$$q_{i,\max} = \frac{K_{L,i}}{a_{L,i}} \quad (3)$$

In an attempt to correlate the single component equilibrium data with the multicomponent equilibrium data, the *P*-factor [27] method was used. The *P*-factor model is simplified approach by using a ratio of monolayer capacity $q_{i,\max}$ for the correlation. The method involved modifying the single component solid-phase concentration $q_{i,\max,\mathrm{single}}$ and correlating it with the $q_{i,\max,\mathrm{multi}}$ values of the mixtures. The capacity factor *P* is converted to a dimensionless form by expressing it as a capacity ratio, the *P*-factor, and is shown in Eq. (4):

$$P_i = \frac{q_{i,\max,\mathrm{single}}}{q_{i,\max,\mathrm{multi}}} \quad (4)$$

The values of the capacity factor *P* for different acid dye systems are presented in Table 4. The values of C_e for a pure single component system were divided by the appropriate *P* values and plotted on the experimental isotherm for that particular system:

$$C_{e,i,\mathrm{multi}} = \frac{1}{P_i} C_{e,i,\mathrm{single}} \quad (5)$$

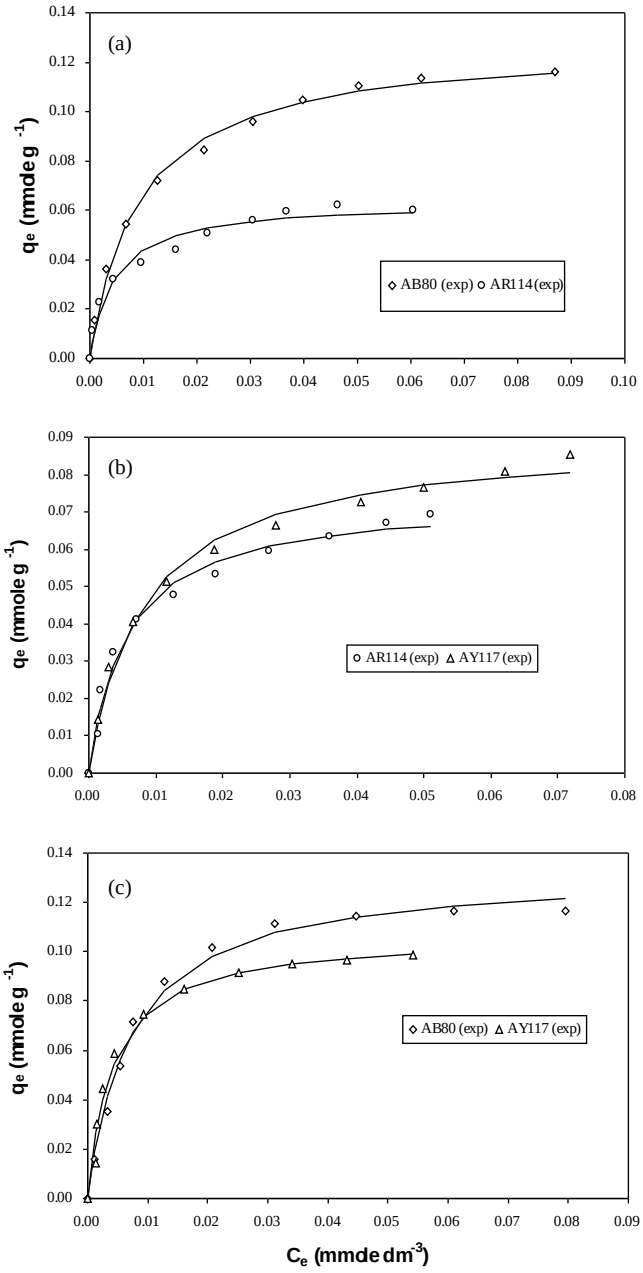

Fig. 3. (a) Langmuir isotherm plots for AB80 and AR114 in a binary system; (b) Langmuir isotherm plots for AB80 and AY117 in a binary system; (c) Langmuir isotherm plots for AR114 and AY117 in a binary system.

$$q_{e,i,\mathrm{multi}} = \frac{1}{P_i} \frac{K^0_{L,i} C_{e,i,\mathrm{single}}}{1 + a^0_{L,i} C_{e,i,\mathrm{single}}} \quad (6)$$

The experimental data points may be correlated with the theoretical data points using Eqs. (5) and (6) and the error analysis based on the SSE, sum of the errors squared, are shown in Table 5. The simplified *P*-factor method does provide a good correlative method. The predicted (solid lines) and experimental data (symbols) are compared in Fig. 5 for the binary equilibrium system, AB80 + AR114.

Table 3
Langmuir isotherm constants and SSE values for AB80, AR114 and AY117 in the single, binary and ternary component systems

	AB80	AR114	AY117			
Single component system						
K_L ($dm^3\,g^{-1}$)	25.68	14.90	40.07			
a_L ($dm^3\,mmol^{-1}$)	101.2	119.2	182.9			
$q_{i,max}$ ($mmol\,g^{-1}$)	0.253	0.125	0.219			
SSE value ($\times 10^{-4}$)	1.524	1.348	2.894			
	AB80 + AR114		AB80 + AY117		AR114 + AY117	
	AB80	AR114	AB80	AY117	AR114	AY117
Binary component system						
K_L ($dm^3\,g^{-1}$)	13.84	14.57	18.27	25.58	13.25	10.98
a_L ($dm^3\,mmol^{-1}$)	108.0	229.2	137.8	239.7	180.4	122.3
$q_{i,max}$ ($mmol\,g^{-1}$)	0.128	0.064	0.133	0.107	0.073	0.090
SSE value ($\times 10^{-4}$)	0.883	1.351	1.344	1.991	0.926	0.684
	AB80 + AR114 + AY117					
	AB80	AR114	AY117			
Ternary component system						
K_L ($dm^3\,g^{-1}$)	50.29	50.02	41.03			
a_L ($dm^3\,mmol^{-1}$)	632.7	949.7	831.8			
$q_{i,max}$ ($mmol\,g^{-1}$)	0.080	0.053	0.049			
SSE value ($\times 10^{-4}$)	0.752	3.657	1.185			

3.2. Rate studies

In order to investigate the mechanism of the adsorption of acid dyes onto activated carbon an intraparticle diffusion based mechanism has been studied. The sorption mechanisms used by other workers involve kinetic based models such as pseudo-first order [28], second-order reversible [29], second-order irreversible [30] and the Elovich model [28]. In the present work, however, for the adsorption of acid dyes, which are large molecules, with long contact times to equilibrium, we consider diffusion-controlled mechanisms are likely to be more appropriate [31]. Diffusional adsorption is usually controlled by an external film resistance and/or internal diffusion mass transport or intraparticle diffusion. Theoretical analysis of intraparticle diffusion yields fairly complex mathematical relationships depending on particle

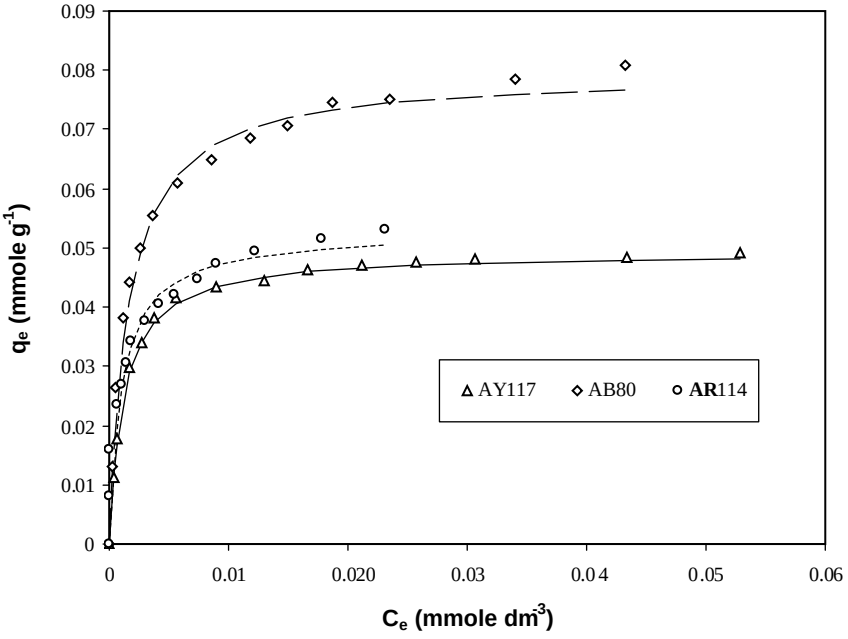

Fig. 4. Langmuir isotherm plots for AB80, AR114 and AY117 in a ternary system.

Table 4
Correlation factor (P) for various acid dye systems

Binary and ternary systems	Acid dyes	Correlation factor, P
AB80 + AR114	AB80	1.977
	AR114	1.953
AB80 + AY117	AB80	1.902
	AY117	2.047
AR114 + AY117	AR114	1.712
	AY117	2.433
AB80 + AR114 + AY117	AB80	3.163
	AR114	2.358
	AY117	4.469

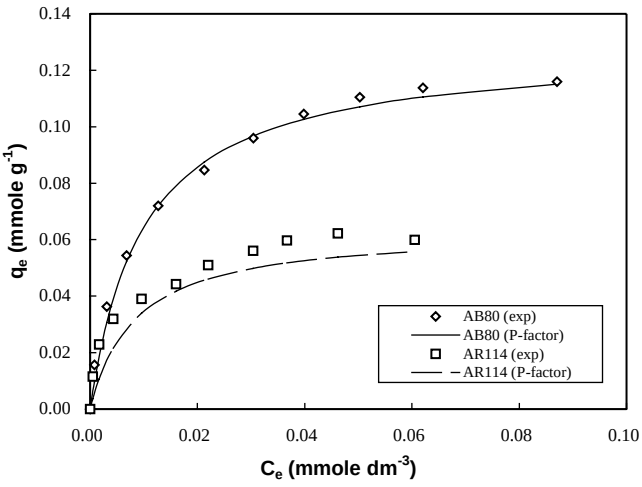

Fig. 5. P-factor analysis plots for AB80 and AR114 in a binary system.

shape. For adsorption onto spherical particles with a constant diffusivity, Crank [32] proposed Eqs. (7) and (8):

$$\frac{q_t}{q_\infty} = 1 - \frac{6}{\pi^2}\sum_{n=1}^{\infty}\frac{1}{n^2}\exp\left(-\frac{n^2\pi^2 D_s t}{r^2}\right) \tag{7}$$

$$\frac{q_t}{q_\infty} = 6\left(\frac{D_s t}{r^2}\right)^{0.5}\left[\frac{1}{\sqrt{\pi}} + 2\sum_{n=1}^{\infty}\mathrm{ierfc}\left(\frac{nr}{\sqrt{D_s t}}\right)\right] - \frac{3D_s t}{r^2} \tag{8}$$

In the earlier stages of the adsorption process, when t is relatively small, Eq. (8) reduces to:

$$q_t = \frac{6q_\infty {D_s}^{0.5}}{\pi^{0.5} r} t^{0.5} \tag{9}$$

which can be represented by Eq. (10):

$$q_t = kt^{0.5} \tag{10}$$

where

$$D_S = \frac{\pi k^2 r^2}{36 q_\infty^2} \tag{11}$$

Furthermore, this solution proposed by Crank [32] is based on the assumption of a linear isotherm. In the present study, the amount of dye adsorbed during the analysis time period of 360 min, is 10–12% of the total capacity. On this basis, the Langmuir equation can be accurately approximated to the linear form:

$$q_{e,i} = K_{L,i} C_{e,i} \tag{12}$$

This equation satisfies the conditions for Eqs. (7) and (8). Eqs. (7) and (10) have been used by a number of workers [11,18,33] in terms of plotting q_t versus time$^{0.5}$ to determine k from the initial linear slopes. McKay and Poots [34] extended the model over longer time periods and identified three linear sections on the root time plot. The authors explained the three sections in terms of pore diameters—macropores, mesopores and micropores.

A plot of the experimental concentration decay curves for the adsorption of AY117 at different initial concentrations are shown in Fig. 6. The plots of q_t versus time$^{0.5}$ are shown in Fig. 7 for the AY117 system for the single component system at different initial concentrations and the values of k are shown in Table 6. The surface diffusivities for three acid dyes at different initial concentration calculated by Eq. (11) are also listed in Table 7.

Fig. 8a and b shows the plots of q_t versus time$^{0.5}$ for the binary system of AB80 and AR114 at different initial dye concentrations. For the ternary system the root time plots are shown in Fig. 9a–c for AB80, AR114 and AY117, respectively, at different initial dye concentrations. The k, D_S and SSE values for the three binary systems and the ternary system are also shown in Tables 6 and 7.

The intraparticle rate parameter plots have been correlated and presented for multicomponent dye adsorption systems. It may be seen that in Fig. 9 and the linearity is still

Table 5
The sum of error square (SSE) values for AB80, AR114 and AY117 in the binary and ternary systems using P-factor analysis

	AB80 + AR114		AB80 + AY117		AR114 + AY117	
	AB80	AR114	AB80	AY117	AR114	AY117
Binary component system						
SSE value ($\times 10^{-4}$)	0.883	1.351	1.344	1.991	0.926	0.684
	AB80 + AR114 + AY117					
	AB80	AR114	AY117			
Ternary component system						
SSE value ($\times 10^{-4}$)	1.385	0.660	3.937			

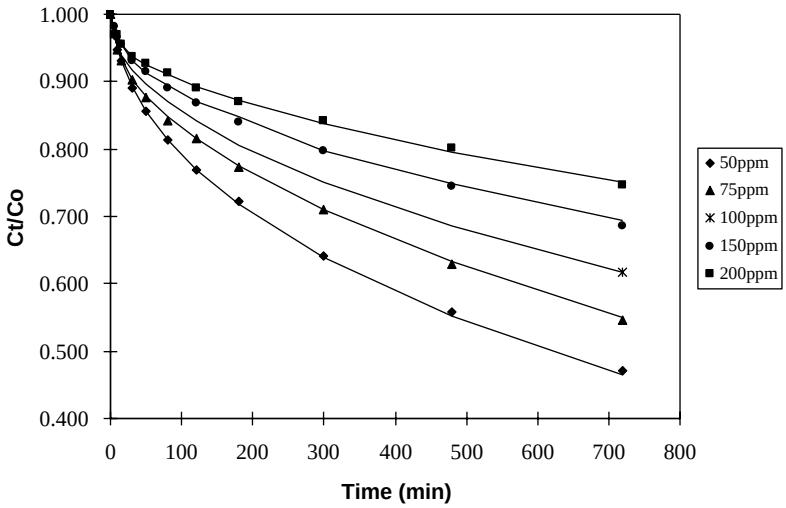

Fig. 6. Plot of the experimental concentration curves for the adsorption of AY117 at different initial concentrations.

maintained for most of the adsorption period. It is important to assess if these results can be used to correlate single component and multicomponent k and D_s values in order to predict multicomponent k and D_s data. It was decided to use the same approach, which we adopted to correlate the equilibrium isotherm data, using the P-factor. For example, the value of the intraparticle rate parameter for AB80 in the AB80/AR114 system ($k_{AB80}^{AB80-AR114}$) can be predicted from single component intraparticle rate parameter (k_{AB80}^{0}) and P-factor value ($P_{AB80}^{AB80-AR114}$) by the following equation:

$$k_{AB80}^{AB80-AR114} = \frac{k_{AB80}^{0}}{P_{AB80}^{AB80-AR114}} \tag{13}$$

and the surface diffusivity of AB80 in AB80 + AR114 mixture can be predicted by Eq. (14):

$$D_{sAB80}^{AB80-AR114} = \frac{D_{sAB80}^{0}}{(P_{Ab80}^{AB80-AR114})^2} \quad \text{since } D_s\alpha\left(\frac{k}{q_\infty}\right) \text{ in Eq. (11)} \tag{14}$$

The predicted intraparticle rate parameters, predicted surface diffusivities and SSE values of the three binary and the ternary systems are presented in Table 8. The data can also be compared graphically by rearranging Eqs. (13) and (14):

$$k_{AB80}^{0} = P_{AB80}^{AB80-AR114} k_{AB80}^{AB80-AR114} \quad \text{or} \quad D_{sAB80,theo}^{0} = (P_{Ab80}^{AB80-AR114})^2 D_{sAB80}^{AB80-AR114} \tag{15}$$

Plots of the experimental single component rate parameters are shown (open symbols), compared with the theoretical single component rate parameters (solid symbols) pre-

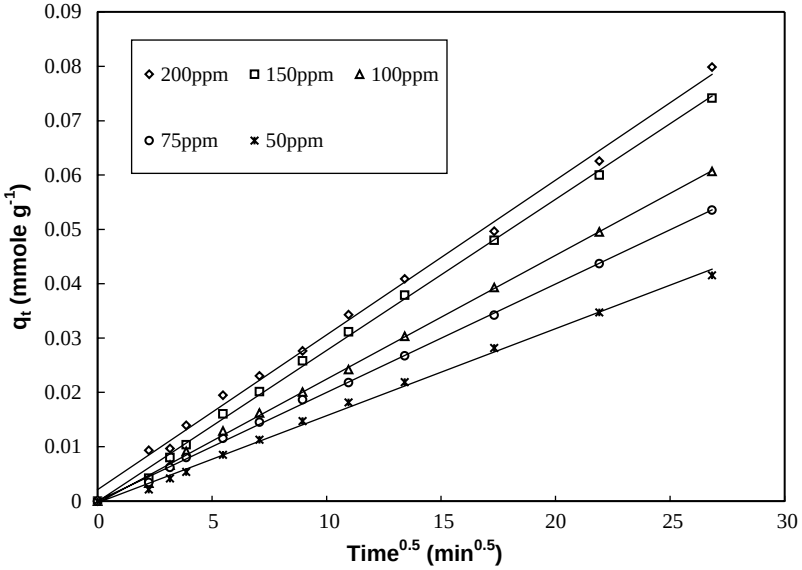

Fig. 7. The q_t vs. time$^{0.5}$ plots for AY117 single component system.

Table 6
Intraparticle rate parameter k for AB80, AR114 and AY117 in the single, binary and ternary component systems

k (1×10^{-3} mmol g^{-1} min$^{-0.5}$)						
	AB80	AR114	AY117			
Single component system						
50 ppm	1.574	0.686	1.692			
75 ppm	1.884	0.908	2.016			
100 ppm	2.248	1.049	2.271			
150 ppm	2.872	1.246	2.610			
200 ppm	3.376	1.402	2.997			
SSE value ($\times 10^{-4}$)	1.380	0.165	0.245			
	AB80 + AR114		AB80 + AY117		AR114 + AY117	
	AB80	AR114	AB80	AY117	AR114	AY117
Binary component system						
50 ppm	0.730	0.269	0.790	0.658	0.369	0.679
75 ppm	1.012	0.374	1.042	0.851	0.475	0.908
100 ppm	1.283	0.473	1.221	1.034	0.545	1.060
150 ppm	1.733	0.641	1.535	1.211	0.675	1.277
200 ppm	2.066	0.786	1.797	1.361	0.767	1.490
SSE value ($\times 10^{-4}$)	0.573	0.023	0.372	0.135	0.059	0.035
	AB80 + AR114 + AY117					
	AB80	AR114	AY117			
Ternary component system						
50 ppm	0.541	0.237	0.371			
75 ppm	0.693	0.298	0.458			
100 ppm	0.861	0.408	0.544			
150 ppm	1.085	0.532	0.662			
200 ppm	1.308	0.660	0.745			
SSE value ($\times 10^{-4}$)	0.153	0.012	0.740			

Table 7
Diffusivities for AB80, AR114 and AY117 in the single, binary and ternary component systems

D_s (1×10^{-10} cm^2 s^{-1})						
	AB80	AR114	AY117			
Single component system						
50 ppm	0.515	0.401	0.795			
75 ppm	0.738	0.702	1.128			
100 ppm	1.051	0.937	1.431			
150 ppm	1.715	1.323	1.891			
200 ppm	2.370	1.674	2.493			
	AB80+AR114		AB80 + AY117		AR114 + AY117	
	AB80	AR114	AB80	AY117	AR114	AY117
Binary component system						
50 ppm	0.111	0.062	0.130	0.120	0.116	0.128
75 ppm	0.213	0.119	0.226	0.201	0.192	0.229
100 ppm	0.342	0.191	0.310	0.297	0.253	0.312
150 ppm	0.625	0.350	0.490	0.407	0.388	0.452
200 ppm	0.888	0.526	0.672	0.514	0.501	0.616
	AB80 + AR114 + AY117					
	AB80	AR114	AY117			
Ternary component system						
50 ppm	0.061	0.048	0.038			
75 ppm	0.100	0.076	0.058			
100 ppm	0.154	0.142	0.082			
150 ppm	0.245	0.241	0.122			
200 ppm	0.356	0.371	0.154			

Table 8
Predicted intraparticle rate parameter and surface diffusivity for AB80, AR114 and AY117 in the binary and ternary component systems

k_{theo} (1×10^{-3} mg g^{-1} min$^{-0.5}$)						
	AB80 + AR114		AB80 + AY117		AR114 + AY117	
	AB80	AR114	AB80	AY117	AR114	AY117
Binary component system						
50 ppm	0.795	0.349	0.822	0.823	0.403	0.693
75 ppm	0.952	0.462	0.985	0.982	0.534	0.826
100 ppm	1.135	0.533	1.175	1.106	0.663	0.930
150 ppm	1.451	0.634	1.501	1.271	0.732	1.069
200 ppm	1.705	0.713	1.765	1.459	0.823	1.228
SSE value ($\times 10^{-4}$)	1.045	0.219	0.288	0.934	0.176	1.036
	AB80 + AR114 + AY117					
	AB80	AR114	AY117			
Ternary component system						
50 ppm	0.500	0.292	0.398			
75 ppm	0.599	0.386	0.474			
100 ppm	0.714	0.446	0.534			
150 ppm	0.913	0.529	0.613			
200 ppm	1.073	0.596	0.704			
SSE value ($\times 10^{-4}$)	1.495	0.159	0.078			
$D_{s,theo}$ (1×10^{-10} cm^2 s^{-1})						
	AB80 + AR114		AB80 + AY117		AR114 + AY117	
	AB80	AR114	AB80	AY117	AR114	AY117
Binary component system						
50 ppm	0.131	0.104	0.141	0.188	0.138	0.133
75 ppm	0.188	0.182	0.202	0.267	0.242	0.189
100 ppm	0.268	0.242	0.287	0.339	0.323	0.240
150 ppm	0.437	0.342	0.469	0.448	0.456	0.317
200 ppm	0.605	0.433	0.648	0.591	0.578	0.418
	AB80 + AR114 + AY117					
	AB80	AR114	AY117			
Ternary component system						
50 ppm	0.052	0.072	0.044			
75 ppm	0.075	0.127	0.062			
100 ppm	0.106	0.169	0.079			
150 ppm	0.173	0.239	0.104			
200 ppm	0.239	0.303	0.138			

dicted using Eq. (15), namely, $k^0_{AB80,theo}$, $k^0_{AR114,theo}$ and $k^0_{AY117,theo}$ in Fig. 10a–c. The equations of the correlative lines in Fig. 10a–c can be correlated by equations of the following type:

$$k = AC_0{}^B \quad (16)$$

Eq. (16) can be transformed to a linear equation (17):

$$\ln(k) = \ln(A) + B\ln(C_0) \quad (17)$$

The three relationships are shown in Eqs. (18)–(20) for the three single component systems AB80, AR114 and AY117 dye and the correlation coefficients are 0.997, 0.985 and 0.998, respectively:

$$k^0_{AB80} = 1.715 \times 10^{-4} C_0{}^{0.561} \quad (18)$$

$$k^0_{AR114} = 0.989 \times 10^{-4} C_0{}^{0.505} \quad (19)$$

$$k^0_{AY117} = 3.502 \times 10^{-4} C_0{}^{0.404} \quad (20)$$

Similar equations have been developed for single component only basic dye adsorption systems [17].

The single correlated lines through all the data points are shown by the single solid line in Fig. 10a–c for each dye in single, binary and ternary systems. The values are close to 0.5 but two are higher. The theoretical equations for intraparticle diffusion indicates that the concentration dependence of a diffusion–adsorption process will vary depending on the characteristics of the adsorption isotherm and on the fraction of solute adsorbed at equilibrium. In the case when only intraparticle diffusion was the rate determining step it was found that k varied with the square root of the initial

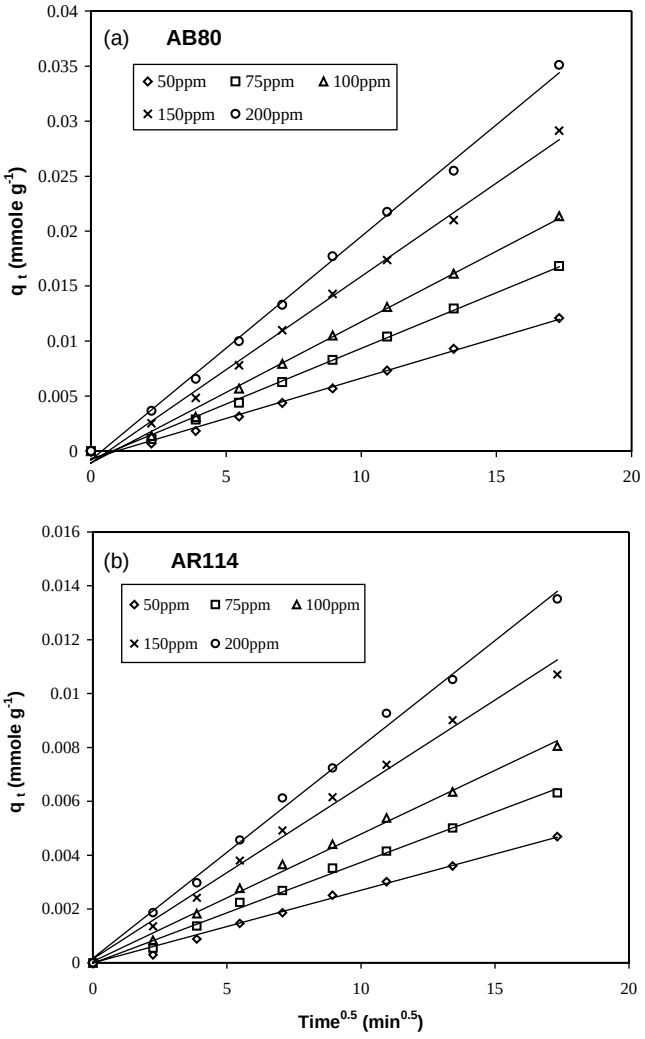

Fig. 8. The q_t vs. time$^{0.5}$ plots for (a) AB80 and (b) AR114 in AB80 + AR114 binary component system.

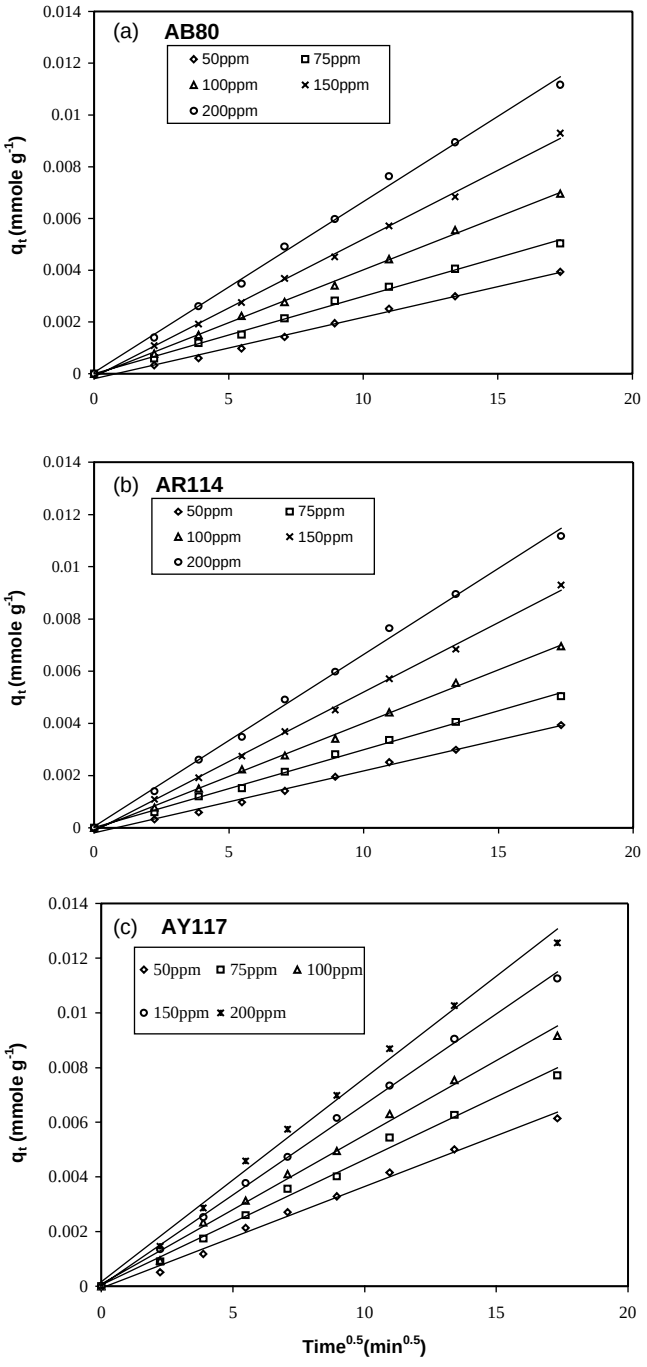

Fig. 9. The q_t vs. time$^{0.5}$ plots for (a) AB80, (b) AR114 and (c) AY117 in AB80 + AR114 + AY117 ternary component system.

concentration used. Previous work by Weber and Morris [35] on single component systems indicated an ideal value of 0.5 for the exponent *B*, which was obtained for the adsorption of alkylbenzene sulphonates on activated carbon. The same mechanism was postulated as a rate-controlling step during the uptake of other solutes by different types of granular adsorbents, including carbon [36].

In the present systems, using the correlated line from single and multicomponent systems, the values are reasonably close to this ideal value, i.e. 0.635, 0.640 and 0.496 for AB80, AR114 and AY117, respectively. The discrepancies may occur for a number of reasons:

Acid dyes in solution will exhibit some degree of ionization, so there may be some solution interactions or activities.

All dyes have the ability to agglomerate and form micelles or clusters of dye molecules of varying molecular weights.

Since the dyes are moderately large molecules they may block some of the carbon micropores thus inhibiting the ideal diffusion behaviour.

Activated carbon is a heterogeneous adsorbent with a wide range of pore sizes and varying surface activities and energies.

These factors would account for the deviation of the concentration exponent from its ideal value of 0.5. Furthermore, in the multicomponent systems, competition and interactions between the different solutes both on the carbon surface and in solution, can occur.

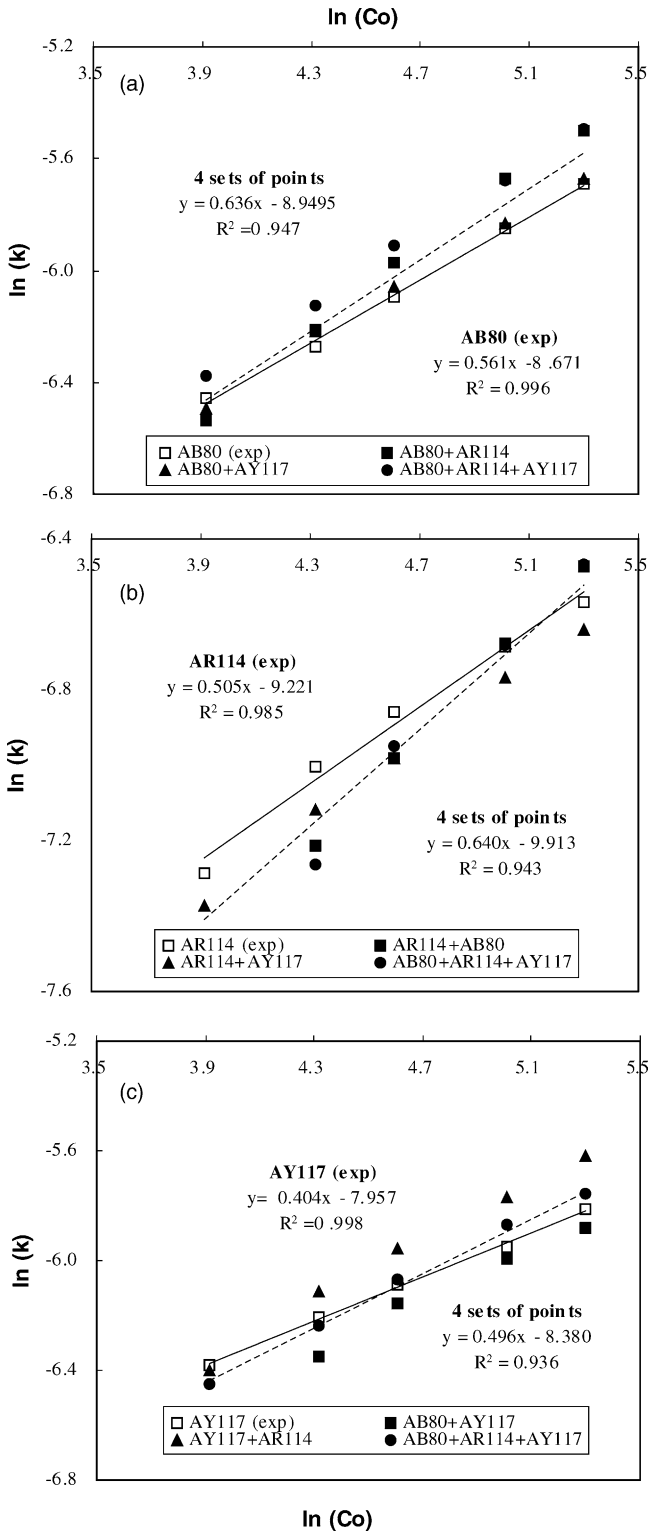

Fig. 10. The ln(k) vs. ln(C_0) plots for (a) AB80, (b) AR114 and (c) AY117.

Furthermore, a comparison of using intraparticle rate parameter (k^0_{dye}) and theoretical single component rate parameters ($k^0_{dye,theo}$) to predict the adsorption uptake curves of three acid dyes onto activated carbon has been shown in

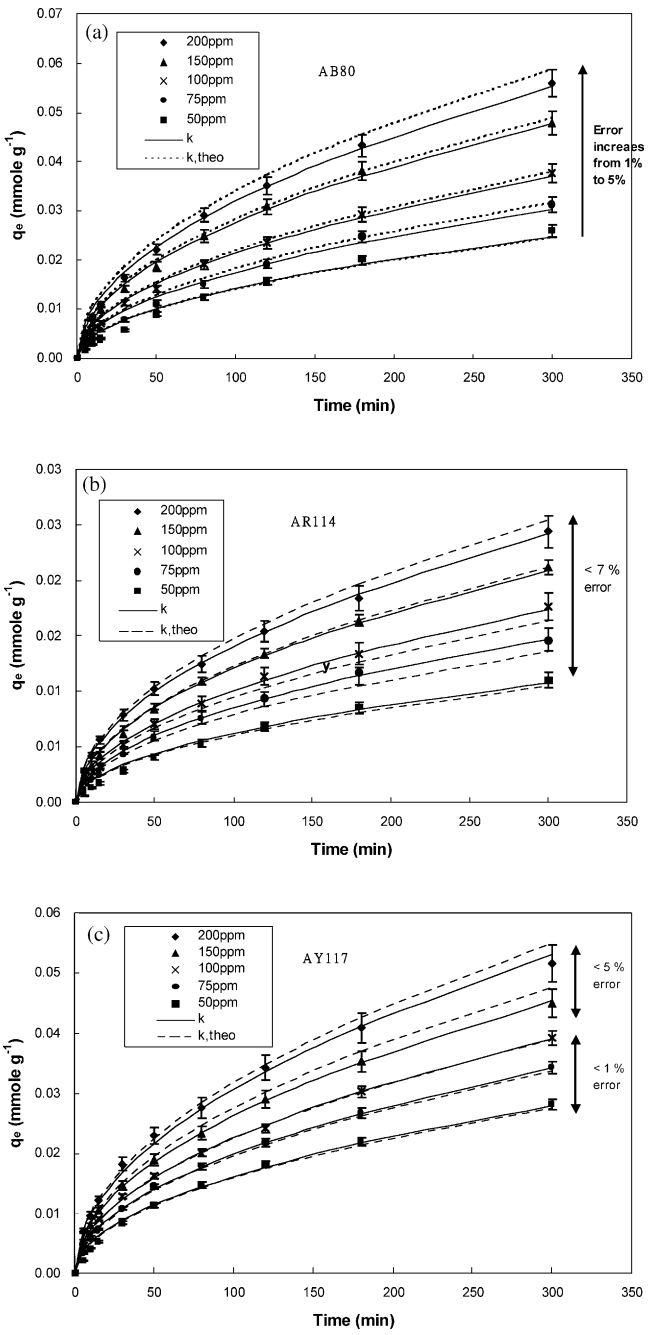

Fig. 11. The comparison of using k and k_{theo} values in the intraparticle diffusion model to predict the adsorption uptake curves of (a) AB80, (b) AR114 and (c) AY117 onto activated carbon at different initial concentrations.

Fig. 11a–c. The prediction results based on $k^0_{dye,theo}$ parameters are reasonably good for all different initial concentration variations in three acid dye systems. The results at low initial concentrations show good agreement between theoretical and experimental values. Although the intraparticle diffusion model using $k^0_{dye,theo}$ parameters at the high dye concentration systems is over-predicting the uptake of dyes onto activated carbon, the error between the experimental and theoretical data is less than 7%. This Crank model has

been developed with the assumption that is only valid during the early stages of adsorption and also assumes a linear isotherm. The lower curves in Fig 11a–c, indicating lower adsorption capacity and a closer approximation to a linear isotherm condition, represent data points with less than 10% adsorbent adsorption capacity. The errors in the fits compared with experimental data are less than 1%, indicating an extremely high level of correlation. For the upper curves in Fig 11a–c, the correlation level is still quite good at less than 7% error disagreement between experimental data and theoretical model results. But the consistently increasing discrepancy is an indication that the model is becoming less effective error at correlating the experimental results as the adsorption capacity increases. Overall, the model proved to be effective for predicting the uptake curves of the acid dye adsorption systems.

4. Conclusion

The adsorption of three acid dyes AB80, AR114 and AY117, onto activated carbon has been studied as three single, three binary and on ternary component system. Equilibrium isotherms have been measured and the Langmuir isotherm constants determined. The monolayer saturation capacities are 0.253, 0.125 and 0.219 mmol g^{-1} carbon for AB80, AR114 and AY117, respectively. Analysis of the rate data has been performed by determining the intraparticle diffusion rate parameters and surface diffusivities form the slopes of plots of the amount of dye adsorbed versus the square root of time of the seven systems. The multicomponent and single component rate parameters can be correlated by using the *P*-factor, derived from the Langmuir isotherm equilibrium constants.

Acknowledgements

The authors are grateful to DAG and RGC, Hong Kong SAR, for the provision of financial support during this research programme.

References

[1] S.R. Marc, Asian textile dye makers are a growing power in changing market, C&EN Northeast News Bureau, 1996, pp. 10–12.
[2] W. Chu, C.W. Ma, Quantitative prediction of direct and indirect dye ozonation kinetics, Water Res. 34 (2000) 3153–3160.
[3] A.T. Peter, H.S. Freeman, Physico-chemical Principles of Color Chemistry, Blackie Academic and Professional, London, 1996.
[4] O. Tunay, I. Kabdasli, G. Eremektar, D. Orhon, Color removal from textile wastewaters, Water Sci. Technol. 34 (1996) 9–16.
[5] B.N. Chen, C.W. Hui, G. McKay, Film-pore diffusion modeling and contact time optimization for the adsorption of dyestuffs on pith, Chem. Eng. J. 84 (2001) 77–94.
[6] M.M. Nassar, Y.H. Magdy, Removal of different basic dyes from aqueous solutions by adsorption on palm-fruit bunch particles, Chem. Eng. J. 66 (1997) 223–226.
[7] G. McKay, S.J. Allen, Single resistance mass transfer models for the adsorption of dyes on peat, J. Sep. Process Technol. 4 (1983) 1–7.
[8] S.J. Allen, G. McKay, K.Y.H. Khader, Multi-component sorption isotherms of basic dyes onto peat, Environ. Pollut. 52 (1988) 39–53.
[9] V.K. Gupta, D. Mohan, S. Sharma, M. Sharma, Removal of basic dyes (rhodamine B and methylene blue) from aqueous solutions using bagasse fly ash, Sep. Sci. Technol. 35 (2000) 2097–2113.
[10] G. McKay, V.J.P. Poots, Kinetics and diffusion processes in colour removal from effluent using wood as an adsorbent, J. Chem. Technol. Biotechnol. 30 (1986) 279–292.
[11] G. Atun, G. Hisarli, Adsorption of carminic acid, a dye onto glass powder, Chem. Eng. J. 95 (2003) 241–249.
[12] G.G. Maghami, G.A. Roberts, Studies on the adsorption of anionic dyes on chitosan, Makromol. Chem. 189 (1988) 2239–2243.
[13] B. Smith, T. Koonce, S. Hudson, Decolorizing Dye Wastewater Using Chitosan, American Dyestuff Reporter, October 1993, pp. 18–36.
[14] R. Juang, M. Chen, Application of the Elovich equation to the kinetics of metal sorption with solvent-impregnated resins, Ind. Eng. Chem. Res. 36 (1997) 813–820.
[15] H. Yoshida, N. Kishimoto, T. Kataoka, Adsorption of glutamic acid on polyaminated highly porous chitosan equilibria, Ind. Eng. Chem. Res. 34 (1995) 347–355.
[16] G.M. Walker, L.R. Weatherley, Prediction of bisolute dye adsorption isotherms on activated carbon, Trans. Inst. Chem. Eng. B 78 (2000) 219–223.
[17] X.Y. Yang, B. Al-Duri, Application of branched pore diffusion model in the adsorption of reactive dyes on activated carbon, Chem. Eng. J. 83 (2001) 15–23.
[18] C.C. Lin, H.S. Liu, Adsorption in a centrifugal field: basic dye adsorption by activated carbon, Ind. Eng. Chem. Res. 39 (2000) 161–167.
[19] G.M. Walker, L.R. Weatherley, Adsorption of dyes from aqueous solution—the effect of adsorbent pore size distribution and dye aggregation, Chem. Eng. J. 83 (2001) 201–206.
[20] G.S. Luo, W.B. Jiang, Y.Y. Dai, Two-phase electrophoresis separation of dyestuffs from dilute solution, Chem. Eng. J. 73 (1999) 37–141.
[21] G. McKay, B. Al-Duri, Extended empirical Freundlich isotherm for binary systems: a modified procedure to obtain the correlative constants, Chem. Eng. Process 29 (1991) 133–138.
[22] S. Rio, A. Delebarre, V. Hequet, P. Le Cloirec, J. Blondin, Metallic ion removal from aqueous solutions by fly ashes: multicomponent studies, J. Chem. Technol. Biotechnol. 77 (2002) 382–388.
[23] K.K.H. Choy, J.F. Porter, G. McKay, Langmuir isotherm models applied to the multicomponent sorption of acid dyes from effluent onto activated carbon, J. Chem. Eng. Data 45 (2000) 575–584.
[24] T. Furusawa, J.M. Smith, Fluid-particle and intraparticle mass transport rates in slurries, Ind. Eng. Chem. Fund. 12 (1973) 197–203.
[25] G. McKay, M. El Geundi, M.M. Nassar, Pore diffusion during the adsorption of dyes onto bagasse pith, Trans. IChemE 74 (1996) 277–288.
[26] I. Langmuir, The adsorption of gases on plane surfaces of glass, mica and platinum, J. Am. Chem. Soc. 40 (1918) 1361–1403.
[27] G. McKay, B. Al-Duri, Simplified model for the equilibrium adsorption of dyes from mixtures using activated carbon, Chem. Eng. Process 22 (1987) 145–156.
[28] C.W. Cheung, J.F. Porter, G. McKay, Elovich equation and modified second-order equation for sorption of cadmium ions onto bone char, J. Chem. Technol. Biotechnol. 75 (2000) 963–970.
[29] Y.S. Ho, G. McKay, The kinetics of sorption of basic dyes from aqueous solution by sphagnum moss peat, Can. J. Chem. Eng. 76 (1998) 822–827.
[30] E.H. Smith, Batch uptake kinetics of cadmium by a recycled iron sorbent, Sep. Sci. Technol. 33 (1998) 149–168.
[31] Y.S. Ho, J.C.Y. Ng, G. McKay, Kinetics of pollutant sorption by biosorbents: review, Sep. Purif. Meth. 29 (2000) 189–232.
[32] J. Crank, The Mathematics of Diffusion, 2nd ed., Clarendon Press, Oxford, 1979.

[33] B. Koumanova, P. Peeva, S.J. Allen, Variation of intraparticle diffusion parameter during adsorption of *p*-chlorophenol onto activated carbon made from apricot stones, J. Chem. Technol. Biotechnol. 78 (2003) 582–587.
[34] G. McKay, V.J.P. Poots, Kinetics and diffusion processes in colour removal from effluent using wood as an adsorbent, J. Chem. Technol. Biotechnol. 30 (1980) 279–282.
[35] W.J. Weber Jr., J.C. Morris, Preliminary appraisal of advanced waste treatment processes, Proc. Int. Conf. Adv. Water Pollut. Res. 2 (1963) 231–241.
[36] F.J. Edeskuty, N.R. Amundson, Effect of intraparticle diffusion, Ind. Eng. Chem. 44 (1952) 1698–1705.